



On mean flow universality of turbulent wall flows. II. Asymptotic flow analysis

Stefan Heinz

Mathematics Department, University of Wyoming, Laramie, WY, USA

ABSTRACT

Understanding of the structure of turbulent flows at extreme Reynolds numbers (Re) is relevant because of several reasons: almost all turbulence theories are only valid in the high Re limit, and most turbulent flows of practical relevance are characterized by very high Re . Specific questions about wall-bounded turbulent flows at extreme Re concern the asymptotic laws of the mean velocity and turbulence statistics, their universality, the convergence of statistics towards their asymptotic profiles, and the overall physical flow organization. In extension of recent studies focusing on the mean flow at moderate and relatively high Re , the latter questions are addressed with respect to three canonical wall-bounded flows (channel flow, pipe flow, and the zero-pressure gradient turbulent boundary layer). Main results reported here are the asymptotic logarithmic law for the mean velocity and corresponding scale-separation laws for bulk flow properties, the Reynolds shear stress, the turbulence production and turbulent viscosity. A scaling analysis indicates that the establishment of a self-similar turbulence state is the condition for the development of a strict logarithmic velocity profile. The resulting overall physical flow structure at extreme Re is discussed.

ARTICLE HISTORY



Received 12 May 2018
Accepted 2 March 2019


KEYWORDS

Wall-bounded turbulent flows; extreme Re ; mean flow and turbulence structure

1. Introduction

Investigations of the structure of turbulent flows at extreme Reynolds numbers are important due to several reasons [1–6]. Such flows are characterized by a large separation of scales between the largest and smallest turbulent motions, so their study offers the best chance to understand the mathematical physical structure of wall-bounded turbulent flows. Correspondingly, almost all theories of turbulence are valid only in the high Reynolds number limit [6]. In addition, most turbulent flows of practical relevance are characterized by very high Reynolds numbers. To develop and to evaluate the performance of computational simulation methods (like large-eddy simulation (LES) [7–12] and hybrid dynamic LES methods [13–20]) for such flows, we need to understand the structure of turbulent flows at extreme Reynolds numbers.

CONTACT Stefan Heinz  heinz@uwyo.edu  Mathematics Department, University of Wyoming, Laramie, WY 82071, USA

 Supplemental data for this article can be accessed here. <https://doi.org/10.1080/14685248.2019.1593425>

Specific problems in this regard concern, for example,

- (P1) Asymptotic Laws: Which self-similar flow structure is established for extreme friction Reynolds numbers Re_τ (how much differ asymptotic and lower Re_τ profiles)?
- (P2) Scaling: How do flow statistics converge to the asymptotic state depending on Re_τ (is the Re_τ scaling of different variables comparable; how are turbulence self-similarity and the log-law onset related)?
- (P3) Physics: How is the flow physically organized at extreme Re_τ (inner-outer scale interactions [21,22]; interaction of streamwise and wall-normal turbulent motions [23,24])?

A basis for addressing the latter questions was provided by a recent identification of the physics of the mean flow structure of several wall-bounded turbulent flows [25] based on recent direct numerical simulation (DNS) and experimental data [26–39]. This study resulted in analytical conclusions about the mean flow structure, its universality and the mechanism of flow-dependent features [25]. Technically, the basic goal of this paper is to extend this analysis, first, by the inclusion of the Reynolds shear stress (which allows conclusions about relevant turbulence characteristics like the turbulent viscosity and turbulence production), and, second, by an analysis of asymptotic features of the mean velocity and Reynolds shear stress for the same three wall-bounded turbulent flows as considered before [25]. One main focus of these studies is on the appearance, universality and extent (the start and end of the log-law) of logarithmic mean velocity variations and their relationship to corresponding laws for turbulence characteristics (the Reynolds shear stress, turbulent viscosity and turbulence production, the production-to-dissipation ratio of turbulent kinetic energy, and the correlation of wall-normal and streamwise turbulent motions). Another main focus is on the better physical understanding of the overall flow organization, the relationship of active and inactive turbulence [22,40–43], inner-outer scale interactions [21,22] and the interaction of streamwise and wall-normal turbulent motions [23,24].

The paper is organized in the following way. Section 2 introduces the mean velocity model presented in Ref. [25] and a corresponding analytical model for the Reynolds shear stress. The problems P1, P2, and P3 described above are addressed in Sections 3,4, and 5, respectively. Section 6 summarizes the conclusions obtained.

2. Analytical models considered

The basis for addressing the problems P1, P2, and P3 introduced in Section 1 is provided here by presenting the model for the mean velocity U^+ derived in Ref. [25] in Section 2.1, and a corresponding analytical model for the Reynolds shear stress $\langle u'v' \rangle^+$ in Section 2.2. These models imply further models considered below: models for the bulk velocity $U_b^+ = \int_0^1 U^+ dy$, skin friction coefficient $C_f = 2/U_b^{+2}$, bulk Reynolds number $Re = 2Re_\tau U_b^+$, turbulence production $P^+ = -\langle u'v' \rangle^+ S^+$, and turbulent viscosity $\nu_t^+ = -\langle u'v' \rangle^+ / S^+$. Here, the superscript + refers to inner scaling, and we use $y^+ = Re_\tau y$ for the inner scaling wall distance (y is normalized by δ , which is the half-channel height, pipe radius, or 99% boundary layer thickness with respect to channel flow, pipe flow, and the TBL, respectively). $S^+ = \partial U^+ / \partial y^+$ refers to the characteristic shear rate.

2.1. Mean velocity model

A presentation of the probabilistic velocity model (PVM) that enables its probabilistic interpretation reads [25]

$$U^+ = \kappa^{-1} \ln(K_* Y e^{\kappa U_{\infty}^+}). \quad (1)$$

Here, the von Kármán constant $\kappa = 0.40$, and $U_{\infty}^+ = \kappa^{-1}(\ln Re_{\tau} + C)$ is the center-line/freestream maximum velocity with $C = (2.076, 2.382, 3.261)$ for channel, pipe, and TBL flow. Equation (1) also involves $K_* = y_{\kappa}^{-1} e^{\sigma \kappa U_{1\infty}^+ - C}$ and Y . Here, Y represents a modification of y due to the damping effect of the wall, and K_* represents (via the involvement of σ) a modification of the flow-dependent constant $K = y_{\kappa}^{-1} e^{\kappa U_{1\infty}^+ - C}$ due to wake effects. In $K = y_{\kappa}^{-1} e^{\kappa U_{1\infty}^+ - C}$ we have $y_{\kappa} = 75.8$ and $U_{1\infty}^+ = 15.85$, which implies $K = (0.933, 0.687, 0.285)$ for channel, pipe, and TBL flow, respectively. In the absence of boundary effects we find $K_* = K$ and $Y = y$. A discussion of deviations of K_* and Y from K and y , respectively, can be found in Ref. [25]. An analytical model for the characteristic shear rate $S^+ = \partial U^+ / \partial y^+$ implied by Equation (1) reads

$$S^+ = S_1^+ + S_2^+ + S_3^+ + S_1^{CP} + S_2^{CP}. \quad (2)$$

This equation includes inner-scale contributions

$$S_1^+ = 1 - \left[\frac{(y^+/a)^{b/c}}{1 + (y^+/a)^{b/c}} \right]^c, \quad \kappa y^+ S_2^+ = \frac{1 + h_3/[1 + y^+/h_1]}{1 + y_{\kappa}/(y^+H)}, \quad (3)$$

where $H = 1/[1 + h_1/y^+]^{h_3}$ and $a = 9$, $b = 3.04$, $c = 1.4$, $h_1 = 12.36$, and $h_3 = 6.47$. Equation (2) also includes the contribution S_3^+ due to wake effects, which is defined by Equation (A.20) in Ref. [25]. The additional contributions S_1^{CP} and S_2^{CP} ensure correct outer boundary conditions for pipe and channel flow. These contributions are defined in the Supplementary Material related to Ref. [25]. S_1^{CP} and S_2^{CP} are very small, but they matter regarding the calculation of turbulent viscosities.

For all the three flows considered, the bulk velocity is defined by $U_b^+ = \int_0^1 U^+ dy$. An analytical model for U_b^+ results from the combination of Equations (S.1) and (S.3) in Suppl. S.1. The skin-friction coefficient based on the bulk velocity is $C_f = 2/U_b^{+2}$, and $Re = 2Re_{\tau} U_b^+$ refers to the bulk Reynolds number, which is based on the bulk velocity. These analytical models for U_b^+ , C_f and Re will be referred to below as PVM- U_b , PVM- C_f and PVM- Re , respectively.

One key ingredient of the derivation of the PVM was the modal decomposition of mean velocities via the identification of wall damping and wake effects. Another key ingredient of deriving Equation (1) was the inclusion of governing equations and identification of linear physics regimes related to the modal velocity decomposition. The fact that several model parameters are involved does not imply that the PVM is an empirical model. A thorough discussion of the ability of the PVM to correctly reflect flow physics can be found in Ref. [25], see Sections 3.2–3.4 on observational physics criteria, physics validation, and comparisons with empirical velocity models. A comprehensive comparison of the PVM versus both experimental data and DNS can be found in Appendix B of Ref. [25] with respect to both moderate and high Re_{τ} . The latter comparisons with DNS and experiments reveal an impressive performance of the PVM.

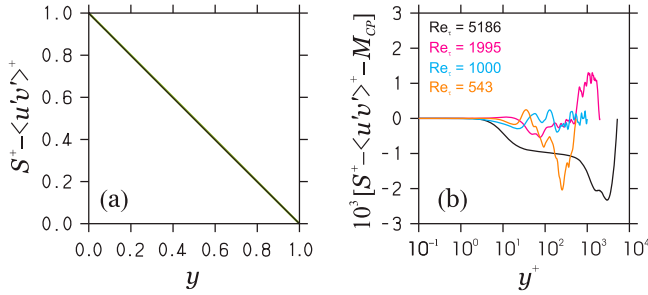


Figure 1. Channel flow: (a) shows $S^+ - \langle u'v' \rangle^+$ obtained from the DNS data of Lee & Moser [26,27] for Re_τ given in (b) in comparison to $M_{CP} = 1 - y$ (thick chartreuse line). Figure (b) shows the relative error of M_{CP} .

2.2. Reynolds shear stress model

The results presented in reference [25] can be extended to the prediction of the Reynolds shear stress $\langle u'v' \rangle^+$ by taking advantage of the momentum balance, $S^+ - \langle u'v' \rangle^+ = M$, where M refers to the total stress and $S^+ = \partial U^+ / \partial y^+$ refers to the characteristic shear rate. The calculation of M is addressed in terms of Figures 1–3, which demonstrate the suitability of $M = M_{CP}$ for channel and pipe flow and $M = M_{BL}$ for the TBL, where

$$M_{CP} = 1 - y, \quad M_{BL} = e^{-y^6 - 1.57y^2}. \quad (4)$$

Here, $M = M_{CP}$ corresponds to the theoretically well-known result for channel and pipe flow, and $M = M_{BL}$ is supported by the DNS data presented here (a theoretical result that explains the structure of $M = M_{BL}$ is unavailable according to the author's knowledge). The most relevant result of Figure 3(a) is given by the fact that the DNS data considered (see the discussion of TBL DNS in reference [25]) collapse very well, this means there is no indication of Reynolds number effects. It has to be noted that this conclusion is based on a limited range of variation of the Reynolds number. Further support for this view arises from (i) the fact that M_{CP} is known to be unaffected by the Reynolds number and (ii) the analysis of the mechanisms of flow effects in reference [25]. The modeling of $\ln M_{BL}$ (instead of M_{BL}) as a polynomial ensures a smooth, non-oscillating decay of M_{BL} . Evidence for the structure of M_{BL} according to Equation (4) is provided by the inset in Figure 3. We see that the initial stage of $\ln M_{BL}$ is a linear function of y^2 . The consideration of a polynomial of third order in y^2 is then appropriate to accurately represent $\ln M_{BL}$. In particular, the model curve closely follows the highest Reynolds number data curve ($Re_\tau = 1989$), which has the smallest relative error: see Figure 3(b). The relative errors related to using Equation (4) are shown in Figures 1(b), 2(b), and 3(b) according to the DNS data considered. It is remarkable that the absolute channel flow error of less than 0.3% is one order of magnitude below the corresponding absolute relative errors of less than 3% for pipe flow and the TBL. In particular, the TBL error, which is slightly smaller than the corresponding pipe flow error, further supports the suitability of $M = M_{BL}$ given by Equation (4).

A corresponding analytical Reynolds shear stress model follows from using $\langle u'v' \rangle^+ = S^+ - M$ in conjunction with Equation (4) for M . The latter relations imply further models. Analytical models for the turbulence production and turbulent viscosity are given by $P^+ = -\langle u'v' \rangle^+ S^+$ and $\nu_t^+ = -\langle u'v' \rangle^+ / S^+$. The models for $\langle u'v' \rangle^+$, P^+ , and ν_t^+ , which are

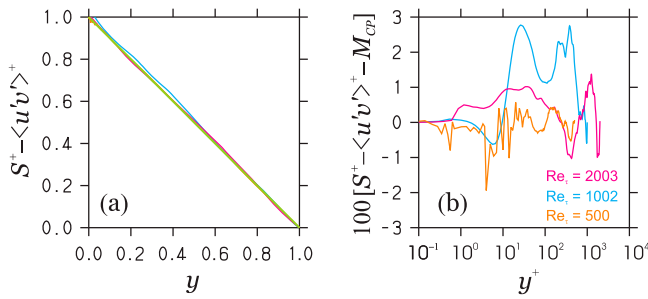


Figure 2. Pipe flow: Figure (a) shows $S^+ - \langle u'v' \rangle^+$ obtained from DNS data of Chin et al. [28] for Re_τ given in (b) compared to $M_{CP} = 1 - y$ (thick chartreuse line). Figure (b) shows the relative error of M_{CP} .

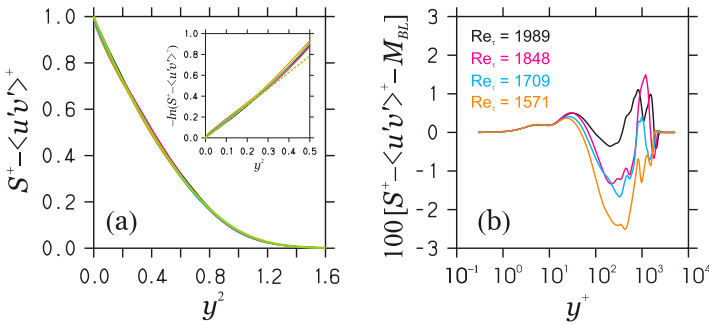


Figure 3. TBL: Figure (a) shows $S^+ - \langle u'v' \rangle^+$ obtained from DNS data of Sillero et al. [29,30] for Re_τ given in (b) compared to $M_{BL} = e^{-y^6 - 1.57y^2}$ (thick chartreuse line). Inset upper right: $-\ln(S^+ - \langle u'v' \rangle^+)$ for relatively small y^2 for the same DNS data. The chartreuse and dashed chartreuse lines shows $1.57y^2 + y^6$ and $1.57y^2$, respectively. Figure (b) shows the relative error of M_{BL} .

directly implied by the PVM, will be referred to below as PVM-UV, PVM-P, and PVM-TV, respectively. Direct evidence for the suitability of $\langle u'v' \rangle^+$ models obtained by involving the momentum balance is given in Figure 4 with respect to the Reynolds shear stress for channel flow, pipe flow, and the TBL. Figures (S.3)–(S.6) in the related Supplementary Material show corresponding direct evidence for the suitability of models for the turbulence production and turbulent viscosity for all three flows considered. In particular, these comparisons present model versus DNS comparisons at the highest Re_τ for which DNS data are available. Corresponding comparisons at lower Re_τ (not shown) demonstrate the same excellent model performance.

An overview of models involved in the discussions below is given in Table 1. The notation PVM-xx, where xx refers to the specific model, is applied to refer to models that are directly implied by the PVM and momentum models. The asymptotic versions of these models at infinite Re_τ are denoted by the subscript ∞ .

3. P1: Asymptotic mean flow and turbulence

The models presented in Section 2 are used now to obtain conclusions regarding problem P1: the asymptotic mean flow and turbulence structure at extreme Re_τ (velocity

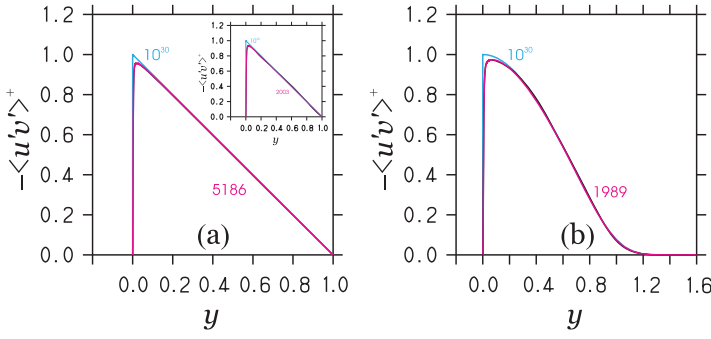


Figure 4. DNS (black lines) versus model (magenta and cyan lines for the given Re_τ) comparisons of Reynolds shear stresses: (a) channel flow DNS data of Lee & Moser [26,27], the upper right inset shows corresponding pipe flow DNS data of Chin et al. [28]; (b) TBL DNS data of Sillero et al. [29,30].

Table 1. Models applied, their asymptotic limits and convergence towards asymptotic limits.

Models	Variables	Section 2: Models	Section 3: Limits	Section 4: Conv.
PVM	$U^+, S^+ = \partial U^+ / \partial y^+$	(1), (2)	see Section 3.1	see Section 4.1
PVM-Ub	$U_b^+ = \int_0^1 U^+ dy$	(S.1), (S.3)	$U_{b\infty}^+$ Eqs. (8)	E_b Equation (17)
PVM-Cf	$C_f = 2/U_b^{+2}$	U_b^+ Equation	$C_{f\infty} = 2/U_{b\infty}^{+2}$	E_b Equation (17)
PVM-Re	$Re = 2Re_\tau U_b^+$	U_b^+ Equation	$Re_\infty = 2Re_\tau U_{b\infty}^+$	E_b Equation (17)
PVM-UV	$\langle u'v' \rangle^+ = S^+ - M$	S^+, M Eq. (4)	$\langle u'v' \rangle_\infty^+$ Equation (9)	E_{uv} Equation (14)
PVM-P	$P^+ = -\langle u'v' \rangle^+ S^+$	$\langle u'v' \rangle^+, S^+$	P_∞^+ Equation (10)	E_p Equation (15)
PVM-TV	$\nu_t^+ = -\langle u'v' \rangle^+ / S^+$	$\langle u'v' \rangle^+, S^+$	$\nu_{t\infty}^+$ Equation (11)	E_ν Equation (16)

Notes: Regarding the PVM, Sections 3.1, 4.1 do not focus on the derivation of asymptotic velocity limits and the related convergence, they focus on the identification and manifestation of the velocity log-law at sufficiently high Re_τ , respectively. The velocity convergence and convergence of other variables are addressed in Figures 6 and 8, respectively.

log-law and subscript ∞ variables, see Table 1). The velocity log-law is considered in Section 3.1, and Section 3.2 deals with a Reynolds shear stress and bulk flow property analysis. Consequences for the bulk velocity, skin-friction coefficient and bulk Reynolds number (which are presented in detail in Suppl. S.1) and turbulence production and turbulent viscosity (which are considered in detail in Suppl. S.2) are summarized in Section 3.2. The convergence towards asymptotic profiles (problem P2) is not considered here but in Section 4.

3.1. Velocity log-law identification

The conclusion of the analysis of the validity of $U^+ = \kappa^{-1} \ln y^+ + B$ (κ refers to the von Kármán constant and B is a constant) for the mean streamwise velocity U^+ in Section II of Ref. [25], which was based on the very accurate channel flows DNS data of Lee & Moser [26,27] at $Re_\tau = 5186$, was that there is no real support for the validity of the log-law [44] at this Re_τ . The question of whether or not there is asymptotically a log-law can be addressed, however, by using the PVM. In absence of boundary effects, the PVM implies that $U^+ = \kappa^{-1} \ln(Ky e^\kappa U_\infty^+) = U_\infty^+ + \kappa^{-1} \ln(Ky)$ is given for all the three flows considered by

$$U^+ = \kappa^{-1} \ln\left(\frac{y^+}{y_\kappa}\right) + U_{1\infty}^+ = \kappa^{-1} \ln y^+ + 5.03, \quad (5)$$

where $K = y_\kappa^{-1} e^{\kappa U_\infty^+ - C}$ and $U_\infty^+ = \kappa^{-1} (\ln Re_\tau + C)$ are applied. An alternative writing of the latter equation is given by the corresponding velocity defect law,

$$U_\infty^+ - U^+ = -\kappa^{-1} \ln\left(\frac{y}{y_\kappa}\right) - U_{1\infty}^+ + \frac{C}{\kappa}. \quad (6)$$

Thus, the PVM implications are fully consistent with the log-law equations $U^+ = \kappa^{-1} \ln y^+ + B$ and $U_\infty^+ - U^+ = -\kappa^{-1} \ln y + B_{def}$, B_{def} being a constant.

In addition to considering the logarithmic limit of U^+ , it is also of interest to consider the extreme velocity limit of U^+ normalized to its centerline/freestream maximum U_∞^+ . Depending on the validity of the mean velocity model $U^+ = \kappa^{-1} \ln y^+ + B + \Pi(y, Re_\tau)$ considered (which neglects variations in the viscous region and considers B and the wake function $\Pi(y, Re_\tau)$ to be not specified), Pullin et al. [5] recently concluded that the local mean velocity must approach the outer velocity for increasing Reynolds numbers at any fixed ratio of the wall-normal location to the outer length scale. By using $U^+ = U_\infty^+ + \kappa^{-1} \ln(Ky)$ and $U_\infty^+ = \kappa^{-1} \ln(e^C Re_\tau)$ we obtain

$$\frac{U^+}{U_\infty^+} = 1 + \frac{\ln(Ky)}{\ln(e^C Re_\tau)}. \quad (7)$$

Hence, in agreement with the assumption of Pullin et al. [5] the PVM predicts a (very slow) convergence of U^+ to U_∞^+ indirectly proportional to $\ln(e^C Re_\tau)$ at infinite Re_τ .

3.2. Asymptotic turbulence and bulk flow properties

To prepare the discussion of the convergence behavior of turbulence and bulk flow properties in Section 4.2, let us consider next the asymptotic profiles of bulk flow variables. As shown in detail in Suppl. S.1, the asymptotic bulk velocities for channel flow, pipe flow, and the TBL are given by

$$U_{b\infty}^+ = \kappa^{-1} \ln(3Re_\tau), \quad U_{b\infty}^+ = \kappa^{-1} \ln(3.52Re_\tau), \quad U_{b\infty}^+ = \kappa^{-1} \ln(5.69Re_\tau), \quad (8)$$

respectively. The latter bulk flow profiles enable the calculation of the asymptotic skin friction coefficient and bulk Reynolds number profiles via $C_{f\infty} = 2/U_{b\infty}^{+2}$ and $Re_\infty = 2Re_\tau U_{b\infty}^+$, respectively. For channel flow, e.g. the relative error of $U_{b\infty}^+$ compared to U_b^+ is (0.64, 0.41, 0.06, 0.007)% for $Re_\tau = (500, 10^3, 10^4, 10^5)$, respectively, see also Figure 8. The relative $C_{f\infty}$ error compared to C_f is twice the $U_{b\infty}^+$ error, and the relative Re_∞ error compared to Re is equal to the $U_{b\infty}^+$ error. A discussion of asymptotic $C_{f\infty}$ and Re_∞ profiles can be found in Suppl. S.1, including a comparison with experimental channel flow data.

The asymptotic features of the Reynolds shear stress $\langle u'v' \rangle^+$ are presented in Figure 4. This figure demonstrates again the excellent model performance by a comparison of model predictions and DNS data for the highest available Re_τ . It also shows model predictions for the almost infinite Reynolds number $Re_\tau = 10^{30}$. It is remarkable that there are relatively minor differences between the DNS data and the extreme Re_τ limit. It can be seen that $\langle u'v' \rangle^+ = -M$ over almost all the flow with an exception of a very narrow near wall region. Figure 5 enables a deeper analysis of these features. The little influence of Reynolds number effects seen in Figure 4 suggests to consider the suitability of approximating the Reynolds

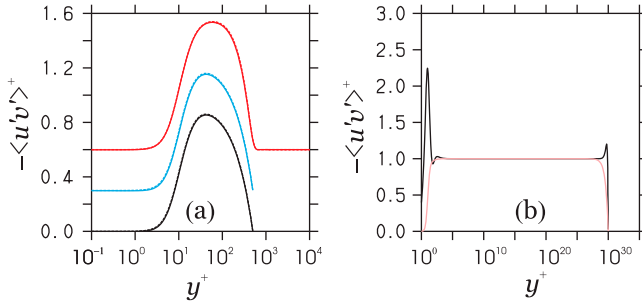


Figure 5. In (a), $\langle u'v' \rangle^+$ according to the PVM-UV (solid lines) and $\langle u'v' \rangle_\infty^+$ (dashed lines) are shown for channel flow (black), pipe flow (blue), and the TBL (red) for $Re_\tau = 500$. Pipe flow and TBL curves are separated by $-\Delta \langle u'v' \rangle^+ = +0.3$. In (b), the modeled Reynolds shear stress (pink lines) for $Re_\tau = 10^{30}$ is compared to $\kappa y^+ S^+$ (black lines) for channel flow.

shear stress by a self-similar asymptotic profile (a product of functions of y^+ and y). The Reynolds shear stress is defined by $-\langle u'v' \rangle^+ = M(1 - S^+/M)$ [25]. Close to the wall, we can approximate the second term by using $M = 1$ and $S^+ = S_1^+ + S_2^+$, where S_1^+ and S_2^+ are given by Equation (3). Correspondingly, we consider the suitability of

$$-\langle u'v' \rangle_\infty^+ = M(1 - S_1^+ - S_2^+). \quad (9)$$

This self-similar relation implies that $-\langle u'v' \rangle_\infty^+/M$ (M is only a function of y) is only a function of y^+ . Figure 5(a) shows that $\langle u'v' \rangle_\infty^+$ approximates $\langle u'v' \rangle^+$ for $Re_\tau = 500$ extremely well for all three flows considered. The difference between $\langle u'v' \rangle_\infty^+$ and $\langle u'v' \rangle^+$ becomes smaller with increasing Re_τ (see Section 4.2). For $Re_\tau \geq 10^4$ there is no visible difference between $\langle u'v' \rangle_\infty^+$ and $\langle u'v' \rangle^+$. The structure of $\langle u'v' \rangle^+$ compared to $\kappa y^+ S^+$ is shown in Figure 5(b) for the extreme $Re_\tau = 10^{30}$ and only for channel flow: corresponding pipe flow and TBL curves are very similar. Like seen regarding the velocity field, the separation of inner (y^+) and outer (y) scalings takes place in the log-layer where $\langle u'v' \rangle^+ = -1$.

The latter results have implications for two relevant combinations of the Reynolds shear stress $\langle u'v' \rangle^+$ and shear rate S^+ : the production $P^+ = -\langle u'v' \rangle^+ S^+$ of turbulent kinetic energy and the turbulent viscosity $\nu_t^+ = -\langle u'v' \rangle^+ / S^+$. A derivation and discussion of the asymptotic production

$$P_\infty^+ = \frac{1}{4} - \left(\frac{1}{2} - [S_1^+ + S_2^+] \right)^2 \quad (10)$$

can be found in Suppl. S.2. Here, S_1^+ and S_2^+ are only functions of y^+ , see Equation (3). A derivation and discussion of the asymptotic ν_t^+ is provided in Suppl. S.2, we find

$$\nu_{t\infty}^+ = C_\mu^\infty \nu_t^{+as}. \quad (11)$$

Equation (11) reflects the separation of inner and outer scaling ($\nu_{t\infty}^+$ is the product of functions of y and y^+). For all the three flows considered, the asymptotic C_μ^∞ reads

$$C_\mu^\infty = \frac{1}{\kappa y^+ (S_1^+ + S_2^+)} - \frac{1}{\kappa y^+}, \quad (12)$$

which is only a function of y^+ . The flow-dependent ν_t^{+as} is $\nu_t^{+as} = \kappa y^+ / G_{CP}$ for channel and pipe flow, and for the TBL, we have $\nu_t^{+as} = \kappa y^+ M_{BL} / G_{BL}$. Here, $M_{BL} = e^{-y^6 - 1.57y^2}$,

and G_{CP} and G_{BL} , which are only functions of y , are defined by [25]

$$G_{CP} = \frac{1 + y + y^2(1.6 + 1.8y)}{Ky + (1 - y)^2(0.6y^2 + 1.1y + 1)}, \quad G_{BL} = \frac{1 + (0.9 + 2y + 3.27y^2)y}{1 + Kyey^{(0.9+y+1.09y^2)}}. \quad (13)$$

For relatively small y , both G_{CP} and M_{BL}/G_{BL} are equal to one. By applying the approximations $G_{CP} = 1$ and $M_{BL}/G_{BL} = 1$, we find $v_t^{+as} = \kappa y^+$, which is the same for all the three flows considered. The relation $v_t^{+as} = \kappa y^+$ simply results from the log-layer scaling of S^+ . This means, the use of $v_t^{+as} = \kappa y^+$ corresponds to the neglect of wake effects. The result $v_t^{+as} = \kappa y^+$ can be also written dimensionally as $v_t^{as} = \kappa \delta y u_\tau$ or $v_t^{as} = \ell_m u_\tau$, where $\ell_m = \kappa \delta y$ refers to a mixing length scale [45].

4. P2: Mean flow and turbulence convergence

Next, the problem P2 described in the introduction will be addressed, this means we ask how mean flow and turbulence properties converge to their asymptotic profiles. In particular, the manifestation of the velocity log-law will be considered in Section 4.1, and the convergence of turbulence and bulk flow properties will be addressed in Section 4.2.

4.1. Velocity log-law manifestation

Let us consider the manifestation of the velocity log-law with increasing Reynolds numbers. This will be done in the next three paragraphs by considering velocity structure changes depending on Re_τ , the extent of $\kappa y^+ S^+$ variations, and implications regarding the extent of the log-law region.

First, let us begin with a discussion of the question of how the structure of the PVM changes with Re_τ . Figure 6(a) presents $\kappa y^+ S^+$ according to the analytical shear model for the three flows considered for $Re_\tau = (10^4, 10^5, 10^6)$, a Re_τ range which covers the highest Re_τ involved in the comparisons presented in reference [25]. Here, $\kappa y^+ S^+$ serves as log-law indicator: $\kappa y^+ S^+ = 1$ reflects the log-law, which can be obtained by integration. Deviations from $\kappa y^+ S^+ = 1$ appear due to velocity variations in the viscous sublayer/buffer layer and the wake region (see also Figure 6(b) for better clarity). Velocity variations in the viscous sublayer/buffer layer are attached to the wall: unaffected by Re_τ they scale with y^+ . Velocity variations in the wake region can be considered to be attached to the centerline/freestream: a plot versus y shows that these variations take place in the same y region independent of Re_τ . The differences seen in Figure 6(a) for different Re_τ result from a shift along the $\ln y^+$ axis according to Re_τ . Due to the increasing separation of velocity variations in the viscous sublayer/buffer layer and the wake region, an increasing Re_τ leads to an increasing plateau region of $\kappa y^+ S^+$ with values close to 1. For a much larger range of Re_τ , Figure 7 shows U^+ and $\kappa y^+ S^+$ for the three flows considered up to extreme Re_τ . The TBL model curves are plotted up to $y = e^3$. This figure shows that the trends seen in Figure 6(a) simply continue for higher Re_τ without any change: the overlap region becomes larger and larger, and velocity variations in the viscous sublayer/buffer layer and the wake region are attached to the wall and centerline/freestream. Wake effects do not disappear: the wake effect is small with respect to channel and pipe flow, but present.

Second, let us continue the discussion in the preceding paragraph with an attempt to quantify the extent of $\kappa y^+ S^+$ variations. This question is addressed in terms of Figure 6(b),

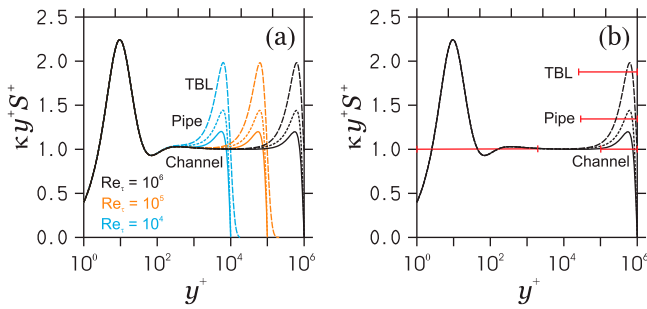


Figure 6. The log-law indicator $\kappa y^+ S^+$ obtained from the PVM is shown in (a) for the given Re_τ and the three flows considered (channel flow: solid line; pipe flow: short dashes; TBL: long dashes). In (b), only the $Re_\tau = 10^6$ curves are shown. The red bars indicate the range of velocity variations in the viscous sublayer/buffer layer (left) and the wake region (right).

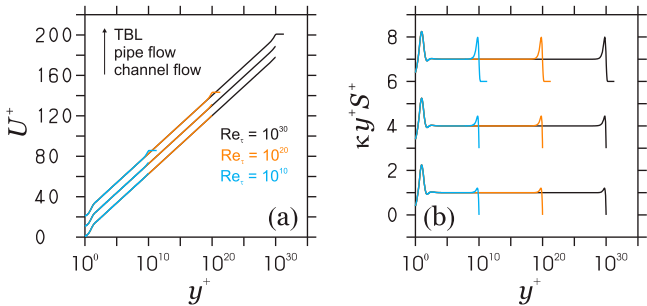


Figure 7. U^+ and $\kappa y^+ S^+$ according to the PVM are shown in (a) and (b), respectively, for channel flow, pipe flow, and the TBL for the given Re_τ . In Figure (a), the data are separated by $\Delta U^+ = 10$. In Figure (b), the data are moved up by +3 and +6 for pipe flow and the TBL, respectively.

which shows for better clarity only the $Re_\tau = 10^6$ curves. Different criteria may be applied to quantify the spatial extent of $\kappa y^+ S^+$ variations in the wake region. After about one decade (illustrated by the red horizontal bar on the right-hand side in Figure 6(b)), $\kappa y^+ S^+$ differs from one by less than 1% for channel flow. So we will use one decade to quantify the spatial variation of wake effects for channel flow. By using the same criterion (a deviation of $\kappa y^+ S^+$ from one by less than 1%) we find for pipe flow and the TBL spatial extents of about 1.5 and 1.6 decades, respectively. The corresponding horizontal bars are also shown in Figure 6(b). By using again a deviation of less than 1%, we find a spatial variation over 3.3 decades for $\kappa y^+ S^+$ variations in the viscous sublayer/buffer layer. The corresponding horizontal bar (which ends at about $y^+ = 2000$) is also shown.

Third, the consequence of this discussion is the following. The consideration of DNS data at $Re_\tau = 5186$ (ranging over $\ln(5186)/\ln(10) = 3.71$ decades measured from $y^+ = 1$) is insufficient to observe a log-law according to the criteria applied here: for channel flow, e.g. the variations of $\kappa y^+ S^+$ in the viscous sublayer/buffer layer and wake region cover about $3.3 + 1 = 4.3$ decades. This fact explains why the discussion related to $U^+ = \kappa^{-1} \ln y^+ + B$ in reference [25] did not provide support for the validity of the log-law. The highest Re_τ considered for the PVM validation in reference [25] are pipe flow measurements at $Re_\tau \approx 10^5$. With respect to the discussions related to Figure 6, this case

corresponds to the consideration of variations over $\ln(10^5)/\ln(10) = 5$ decades. For this case, the variations of $\kappa y^+ S^+$ in the viscous sublayer/buffer layer and wake region cover about $3.3 + 1.5 = 4.8$ decades. Therefore, this case enables the validation of the log-law, although the range of log-law variation is still less than one decade.

It has to be noted that the criteria for identifying the log-law applied here are very strict. Obviously, by slightly relaxing these criteria, we find a more extended region that behaves log-law-like (the log-law region is sometimes considered to start at $y^+ = 200$ [46], which adds a full decade to the log-law region considered here). In this regard, it is also of interest to refer to the lower log-law bound $3Re_\tau^{1/2}$ considered by Marusic et al. [47]. The authors note that such a scaling contradicts to classical theories, and that the observations presented do not prove the correctness of bounds applied: they are simply used for the purpose of curve fitting the parameters in logarithmic equations. An argument against the lower log-law bound $3Re_\tau^{1/2}$ is the following. By using $3Re_\tau^{1/2}$, the log-law region of channel flow at $Re_\tau = 5186$ would be expected to start at $y^+ = 216$. But Lee and Moser [26] report that there is no log-law region for $Re_\tau = 5186$.

4.2. Convergence of turbulence and bulk flow properties

Let us have a closer look at how mean flow characteristics (the bulk velocity) and turbulence characteristics (the Reynolds shear stress, turbulence production, and turbulent viscosity) converge to an asymptotic state. The main motivation to do so is to see how the development of a logarithmic velocity profile is related to the development of self-similarity of other flow properties. In order to simplify matters, the following discussion will be presented by focusing on channel flow. The corresponding features of pipe flow and the TBL are very similar.

Let us begin with specifying relative deviations to quantify asymptotic convergence. To assess relative deviations of the Reynolds shear stress and turbulence production, we consider first the deviations Δ_{uv} and Δ_P , respectively, between these variables and their asymptotic profiles. It turns out that these variables have maximum values very close to the wall. In this case, we have $\Delta_{uv} = |\langle u'v' \rangle^+ - \langle u'v' \rangle_\infty^+| = |S^+ - M(S_1^+ + S_2^+)| = |S_1^+ + S_2^+ - M(S_1^+ + S_2^+)| = Re_\tau^{-1}F(y^+)$, where $F(y^+) = y^+(S_1^+ + S_1^+)$. It is worth noting that S_2^+ , basically, does not contribute here in comparison to S_1^+ . A corresponding analysis shows that $\Delta_P = |P^+ - P_\infty^+|$ is equal to Δ_{uv} , this means $\Delta_{uv} = \Delta_P$. The analysis of $F(y^+)$ shows that this function has a maximum $F_M = 5.608$ at $y_M^+ = 9.57$. Hence, we find maximum deviations $\Delta_{uv,\max} = \Delta_{P,\max} = F_M/Re_\tau$ at $y^+ = y_M^+$. On this basis, we can define the relative deviation of the Reynolds shear stress in percent by

$$E_{uv} = -\frac{100\Delta_{uv,\max}}{(\langle u'v' \rangle^+)_{y^+=y_M^+}} = \frac{100y_M^+}{(y_M^+/F_M - 1)Re_\tau} = \frac{1355}{Re_\tau}, \quad (14)$$

where $-(\langle u'v' \rangle^+)_{y^+=y_M^+} = 1 - F_M/y_M^+$, and the corresponding relative deviation of the turbulence production is given by

$$E_P = \frac{100\Delta_{P,\max}}{(P^+)_{y^+=y_M^+}} = \frac{100y_M^+}{(1 - F_M/y_M^+)Re_\tau} = \frac{2312}{Re_\tau}. \quad (15)$$

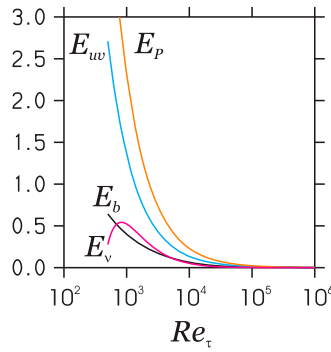


Figure 8. The Re_τ dependence of relative deviations E_{uv} , E_p , E_v , and E_b (see Equations (14)–(17)) of flow characteristics from their self-similar profiles.

Regarding the turbulent viscosity ν_t^+ , it turns out that the largest deviation from its asymptotic profile $\nu_{t\infty}^+ = C_\mu^\infty \nu_t^{+as}$ is found at $y = 1$. At the point $y = 1$, we have $\nu_t^+(1) = \kappa Re_\tau K / 5.4 - 1$ and $\nu_{t\infty}^+(1) = ([S_1^+(1) + S_2^+(1)]^{-1} - 1)K / 5.4$. The corresponding relative error is defined by

$$E_v = 100 \frac{\nu_t^+(1) - \nu_{t\infty}^+(1)}{\nu_t^+(1)}. \tag{16}$$

With respect to mean flow properties, U^+ and, therefore, S^+ do not establish self-similar profiles because they represent superpositions of several contributions. In comparison to the scaling of turbulence characteristics, it is, however, of interest to consider integral velocity characteristics, this means the scaling of how the bulk velocity U_b^+ asymptotically approaches its logarithmic limit $U_{b\infty}^+$ (see the discussion in Suppl. S.1). The relative deviation of the bulk velocity from its logarithmic asymptotic variation in percent reads $E_b = 100|U_b^+ - U_{b\infty}^+|/U_{b\infty}^+$. According to Equations (S.1) and (S.4), we have

$$E_b = \frac{100(I_{12} - 1)}{\ln(3Re_\tau)}. \tag{17}$$

The corresponding relative deviation of the bulk Reynolds number is equal to E_b , and the corresponding relative deviation of the skin-friction coefficient is $2E_b$.

The relative deviations E_b , E_{uv} , E_p , and E_v of flow characteristics are shown in Figure 8 in dependence on Re_τ . For $Re_\tau \geq 20,000$, all these relative deviations are smaller than 0.1%, i.e. the turbulence characteristics have, basically, self-similar profiles, which is reflected regarding the mean flow by a logarithmic variation of the bulk velocity.

The results reported here support for the channel flow considered the following view of overall asymptotic flow variations with Re_τ . At about $Re_\tau = 20,000$, the turbulence characteristics considered here have established self-similar states. According to the discussion in Section 4.1, it needs velocity variations over at least 4.3 decades (measured from $y^+ = 1$) to observe a strict log-law, and $Re_\tau = 20,000$ satisfies this constraint: we have velocity variations ranging over $\ln(20,000)/\ln(10) = 4.3$ decades. These findings indicate that the establishment of a self-similar state implied by the scale separation of inner and

outer scalings is the condition for the development of a strict logarithmic velocity profile. By using corresponding criteria derived for pipe flow and the TBL in Section 4.1 (velocity variations over 4.8 and 4.9 decades, respectively), we may expect that corresponding critical Reynolds numbers for the observation of a strict log-law for pipe flow and the TBL are given by about $Re_\tau = 63,000$ and $Re_\tau = 80,000$, respectively.

5. P3: Asymptotic flow organization

Let us finally address problem P3: we use findings presented above to obtain a better understanding of the asymptotic physical flow structure. To prepare this discussion, Section 5.1 deals with extensions of results obtained before via a discussion of the turbulence production-to-dissipation ratio and the correlation of streamwise and wall-normal turbulent motions. Implications of observations regarding the understanding of turbulence components and the asymptotic flow structure are discussed in Sections 5.2 and 5.3, respectively.

5.1. Production and correlation balances

Let us address two questions (which can be seen to be related to the use of different normalizations for the Reynolds shear stress), which are closely related to the discussions presented before. In contrast to the analysis above, clarification on these questions requires information in addition to the analytical models presented above (it requires the dissipation rate of turbulent kinetic energy and Reynolds normal stresses).

With respect to the turbulence production P^+ , a very important question is its ratio to the normalized dissipation rate $\varepsilon^+ = \varepsilon v/u_\tau^4$. With respect to channel flow DNS data at the highest available Reynolds number $Re_\tau = 5186$, Lee & Moser [26,27] concluded that there is currently no evidence for the existence of a regime where production and dissipation clearly balance each other. However, relevant conclusions regarding this question can be drawn by taking reference to a recent analysis of ε [48]. In particular, Abe and Antonia considered the matching of ε scalings in an overlap region corresponding to the velocity scaling (see Section II of reference [25]). They concluded that ε scales in this overlap region according to $\varepsilon y \delta / u_\tau^3 = 1/\kappa$ if Re_τ is sufficiently large. It is worth noting that this observation is independent of the existence of a velocity log-law or the assumption of a production-dissipation balance. By taking reference to $Re_\tau = u_\tau \delta / \nu$, the latter scaling can be written $\varepsilon^+ = 1/(\kappa y^+)$. Evidence for this scaling is provided in terms of Figure 9: the $Re_\tau = 5186$ curve in Figure 9(b) demonstrates the correctness of this scaling, and Figure 9(a) shows that the range of applicability of this scaling extends for increasing Re_τ (simultaneously, this figure also illustrates the difficulty to obtain a general analytical expression for ε corresponding to the PVM). The combination of $\varepsilon^+ = 1/(\kappa y^+)$ with the conclusion that P^+ scales in the log-law region with $1/(\kappa y^+)$ leads then to $P^+/\varepsilon^+ = 1$ for sufficiently large Re_τ in the log-law region. This result matters regarding the design of turbulence models that often apply $P^+/\varepsilon^+ = 1$.

Another relevant question concerns the asymptotic structure of the correlation coefficient $\rho_{uv} = \langle u'v' \rangle^+ / (\langle u'u' \rangle^+ \langle v'v' \rangle^+)^{1/2}$, which measures the interaction of streamwise and wall-normal turbulent motions. TBL analyzes support the view that ρ_{uv} decreases

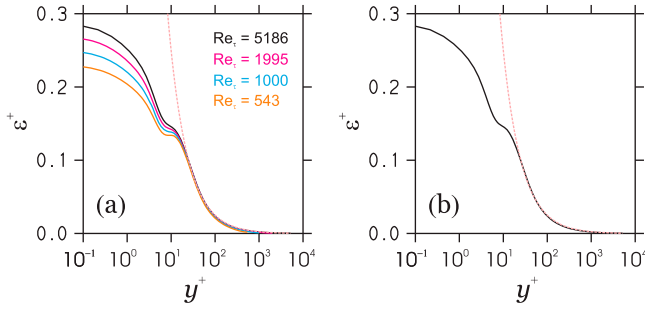


Figure 9. The dissipation rate ε^+ is shown in (a) according to the DNS data of Lee & Moser [26,27] for the given Reynolds numbers. For clarity, only the $Re_\tau = 5186$ curve is shown in (b). In both plots, the dashed pink curves shows the asymptotic scaling $\varepsilon^+ = 1/(\kappa y^+)$.

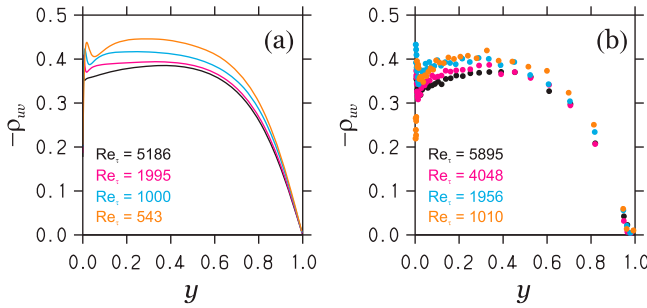


Figure 10. The correlation coefficients $\rho_{uv} = \langle u'v' \rangle^+ / (\langle u'u' \rangle^+ \langle v'v' \rangle^+)^{1/2}$ are shown in (a) according to the channel flow DNS data of Lee & Moser [26,27] and in (b) according to the channel flow experimental data of Schultz & Flack [31] for the given Re_τ .

with an increasing Reynolds number [23,24]. For extreme Re_τ , this would imply a decoupling of streamwise and wall-normal turbulent motions (because of an increasing scale separation between streamwise and wall-normal turbulent velocities). Figure 10 shows the correlation coefficient ρ_{uv} for channel flow according to the very accurate DNS data of Lee & Moser [26,27] and experimental data of Schultz & Flack [31] for the available range of Re_τ . First, this comparison reveals a discrepancy between DNS and experimental data: the experimental data slightly under-predict ρ_{uv} . Second, the Reynolds number effects may indeed support the view that the correlation coefficient decreases with Re_τ . A more detailed view of that can be obtained by considering the factor $(\langle u'u' \rangle^+ \langle v'v' \rangle^+)^{-1/2}$ in $\rho_{uv} = \langle u'v' \rangle^+ / (\langle u'u' \rangle^+ \langle v'v' \rangle^+)^{1/2}$, which is shown in Figure 11. We see again a discrepancy between DNS and experimental data. Although the Reynolds number range is limited, it seems that there is no indication that $(\langle u'u' \rangle^+ \langle v'v' \rangle^+)^{-1/2}$ disappears asymptotically. In particular the close agreement of the highest Re_τ curves supports the view that $(\langle u'u' \rangle^+ \langle v'v' \rangle^+)^{-1/2}$ converges to a nonzero asymptotic distribution. Combined with the asymptotic Reynolds shear stress behavior $-\langle u'v' \rangle_\infty^+ = M(1 - S_1^+ - S_2^+)$, see Equation (9), it appears that the correlation coefficient converges to a nonzero asymptotic profile. Hence, in correspondence to the local balance of production and dissipation of turbulent kinetic energy in the log-layer, streamwise and wall-normal turbulent motions seem to approach an asymptotic equilibrium state of interaction.

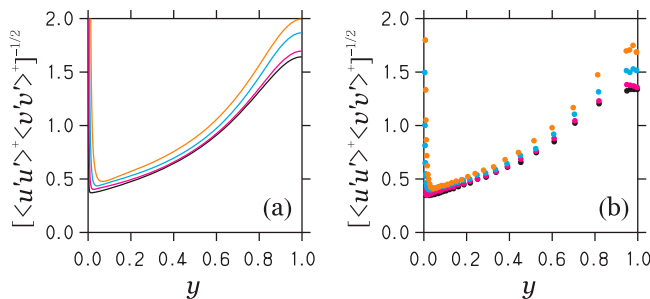


Figure 11. The factors $(\langle u'u' \rangle^+ \langle v'v' \rangle^+)^{-1/2}$ in $\rho_{uv} = \langle u'v' \rangle^+ / (\langle u'u' \rangle^+ \langle v'v' \rangle^+)^{1/2}$ are shown in (a) according to the channel flow DNS data of Lee & Moser [26,27] and in (b) according to the channel flow experimental data of Schultz & Flack [31] by using the same color code as in Figure 10.

5.2. Local and non-local turbulence

Let us try to relate the analytical conclusions reported above to ideas about properties of turbulent motions to accomplish a deeper overall understanding of the asymptotic turbulence structure. The asymptotic similarity laws for the Reynolds shear stress $\langle u'v' \rangle^+$, turbulence production P^+ , and turbulent viscosity ν_t^+ reported here have an interesting property: these turbulence properties appear as products of functions that scale either with $S_1^+ + S_2^+$ or with y . A reasonable concept, which is relatively close to Townsend's ideas of different turbulence components [1,22,40–43,49–53] (see below), is to relate a scaling in $S_1^+ + S_2^+$ to local turbulence (small-scale eddies close to the wall), and a scaling in y to non-local turbulence (large-scale motions extending through all the flow field, they are produced by energetic processes remote from the wall, they scale by involving boundary information). The fact that the asymptotic turbulence similarity laws appear as products of $S_1^+ + S_2^+$ and y means that there is a zero interaction between local and non-local turbulence: y scalings do not affect $S_1^+ + S_2^+$ scalings and vice versa. In particular, the effect of non-local turbulence extends throughout the whole flow field, but it does not affect local turbulence.

It is of interest to compare this view with Townsend's idea of different turbulence components. Townsend's notion can be described as follows [22,40–43,49]. There are two sorts of turbulence in the inner wall region: active and inactive turbulence, and they do not interact. Active turbulence is assumed to contribute all of the Reynolds shear stress $\langle u'v' \rangle^+$. Inactive turbulence is seen as large-scale motion acting in planes parallel to the wall. It contributes to $\langle u'u' \rangle^+$ and $\langle w'w' \rangle^+$, but not to $\langle v'v' \rangle^+$ and $\langle u'v' \rangle^+$ [49]. Nevertheless, this hypothesis was found to disagree with observations [22,43].

The results reported here show that the Reynolds shear stress is not the result of one sort of turbulent motion: it is the result of two sorts of turbulent motions. In particular, the asymptotic Reynolds shear stress $-\langle u'v' \rangle_\infty^+ = M(1 - S_1^+ - S_2^+)$ is affected by both local and non-local turbulence: it is produced by local turbulence $(1 - S_1^+ - S_2^+)$ and decreased by non-local turbulence (via M). Based on the fact that the Reynolds shear stress is produced by local turbulence, we may consider local turbulence as active turbulence. To avoid confusion with Townsend's concept of inactive turbulence, non-local turbulence may be considered then as passive turbulence (with the understanding that it affects $-\langle u'v' \rangle_\infty^+$, but it does not generate it).

5.3. Asymptotic flow structure

The idea of local and non-local turbulence components and their zero interaction presented here is helpful for the better understanding of the overall asymptotic flow structure, as described in the following three paragraphs.

First, if there is no interaction between local and non-local turbulence, it is plausible to find an asymptotic local equilibrium between the production and dissipation of turbulent kinetic energy (turbulent kinetic energy is dissipated close to where it is produced), as indicated by the findings reported in Section 5.1. If production and dissipation of turbulence would not balance each other locally, there would be spatial energy transport that interferes with non-local turbulence. Therefore, local turbulence would affect non-local turbulence in this case, which contradicts to the zero interaction of local and non-local turbulence reported here.

Second, if there is no interaction between local and non-local turbulence, it is also plausible that streamwise and wall-normal turbulent motions approach an asymptotic equilibrium state of interaction, as indicated by the discussion in Section 5.1. If streamwise and wall-normal turbulent motions would be asymptotically decoupled [23,24], it would be impossible to observe an asymptotic local equilibrium of the production and dissipation of turbulent kinetic energy (because there is no production).

Third, if there is no interaction between local and non-local turbulence, it is a requirement to find the same inner-scaled flow statistics in internal flows and boundary layers at the same Reynolds number. This is indeed the case, as it was reported recently [25]. In particular, it was found that flow effects modify non-local turbulence only via absolutely required geometry and domain effects [25]. In other words, non-local turbulence can be seen as a passive set-up determined by the domain and boundary conditions. Hence, the findings reported here and in Ref. [25] combine to one coherent picture of the asymptotic turbulence structure of the three flows considered.

6. Concluding remarks

The understanding of the asymptotic structure of wall-bounded turbulent flows at extreme Re_τ is an important research topic as discussed in Section 1. To further advance our understanding, this paper was focused on three problems: P1 (the structure of asymptotic laws for the mean velocity and related turbulence statistics), P2 (the convergence of mean flow and turbulence statistics towards the asymptotic laws), and P3 (the physical flow organization at extreme Re_τ). The technical approach to address these questions was (i) to extend a recent identification of the mean flow physics of three canonical wall-bounded turbulent flows (channel flow, pipe flow, and the TBL) by corresponding results for the Reynolds shear stress (which allows conclusions for the turbulent kinetic energy production, turbulent viscosity, production-to-dissipation ratio of turbulent kinetic energy and the correlation of streamwise and wall-normal turbulent velocities), and (ii) to analyze asymptotic flow statistics on this basis. It is relevant to note that the analysis of Reynolds shear stress features was performed in the same spirit as analyzing the mean flow in Ref. [25]: it was demonstrated that the analytical models obtained satisfy criteria for veritable physics (see Section 2.2). Detailed answers to the problems P1, P2, and P3 were provided in Sects. 3,4, and 5, respectively. The main findings are summarized in the following.

With respect to P1, the main novelty presented here is the derivation of analytical asymptotic relationships for mean flow and related turbulence variables. The following was concluded.

- (1) There is clear evidence for the validity of the velocity log-law combined with a constant, universal von Kármán constant $\kappa = 0.40$ for the three flows considered.
- (2) With respect to the skin friction coefficient variation, there is no support for a power law variation [54,55]. Instead, the skin friction coefficient follows asymptotically an inverse quadratic logarithmic function (which is an accurate model for $Re_\tau \geq 500$) in line with the friction law.
- (3) Asymptotic, self-similar profiles (products of functions of y^+ and y) were obtained for $\langle u'v' \rangle^+$, P^+ , and v_t^+ (which is an essential ingredient of turbulence models). They may be considered as a reflection of the scale separation, equivalent to the velocity log-law.

With respect to P2, the main novelty presented here is the derivation of the analytical convergence behavior of mean flow and related turbulence variables. The following was concluded.

- (1) The log-law establishment coincides with the establishment of asymptotic turbulence profiles. This supports the view that the establishment of self-similar, scale-separation laws for the turbulence is the condition for the development of a strict logarithmic velocity profile.
- (2) With respect to channel flow, there is a critical $Re_\tau = 20,000$ required to observe a strict log-law. For pipe flow and the TBL, we find critical $Re_\tau = 63,000$ and $Re_\tau = 80,000$, respectively. The relationship to alternative log-law bounds was discussed.
- (3) A relevant observation is the fact that the self-similar turbulence profiles provide already very good approximations for $Re_\tau \geq 500$.

With respect to P3, the main novelty presented here is the explanation of basic asymptotic flow organization features based on the observed zero interaction of local and non-local turbulence. In particular, the following was concluded.

- (1) Asymptotic similarity laws for $\langle u'v' \rangle^+$, P^+ , and v_t^+ reflect a zero interaction between local and non-local turbulence: they coexist without affecting each other. The effect of non-local turbulence extends throughout the whole flow field, but it does not affect local turbulence.
- (2) An asymptotic local equilibrium of the production and dissipation of turbulent kinetic energy and an asymptotic equilibrium state of interaction of streamwise and wall-normal turbulent motions represent reflections of the missing interaction of local and non-local turbulence.
- (3) The findings obtained are consistent with other conclusions reported recently [25]: a zero interaction of local and non-local turbulence is a requirement to find at the same Re_τ the same inner-scaled flow statistics in internal flows and boundary layers.

Acknowledgments

The author is very thankful to the referees for their helpful suggestions for improvements.

Disclosure statement

No potential conflict of interest was reported by the authors.

Funding

The author would like to acknowledge partial support through Langley Research Center (NASA's NRA) research opportunities in aeronautics program (grant number NNX12AJ71A with Dr P. Balakumar as technical officer) and the National Science Foundation (Directorate for Mathematical and Physical Sciences (DMS - CDS&E-MSS), grant number 1622488 with Dr Y. Zeng as Technical Officer). Substantial support from the Hanse-Wissenschaftskolleg, Institute for Advanced Study, Delmenhorst, Germany (Hanse-Wissenschaftskolleg) (Delmenhorst, Germany, Technical Monitor: W. Stenzel) is gratefully acknowledged.

References

- [1] Marusic I, McKeon BJ, Monkewitz PA, et al. Wall-bounded turbulent flows at high Reynolds numbers: recent advances and key issues. *Phys Fluids*. 2010;22(6):065103/1–065103/24.
- [2] Smits AJ, McKeon BJ, Marusic I. High-Reynolds number wall turbulence. *Annu Rev Fluid Mech*. 2011;43(1):353–375.
- [3] Jiménez J. Near-wall turbulence. *Phys Fluids*. 2013;25(10):101302/1–101302/28.
- [4] Wallace JM. Highlights from 50 years of turbulent boundary layer research. *J Turbulence*. 2013;13(53):1–70.
- [5] Pullin DI, Inoue M, Saito N. On the asymptotic state of high Reynolds number, smooth-wall turbulent flows. *Phys Fluids*. 2013;25(1):015116/1–015116/9.
- [6] Hultmark M, Vallikivi M, Bailey SCC, et al. Turbulent pipe flow at extreme Reynolds numbers. *Phys Rev Lett*. 2012;108:094501/1–094501/5.
- [7] Kalitzin G, Medic G, Templeton JA. Wall modeling for LES of high Reynolds number channel flows: what turbulence information is retained?. *Comput Fluids*. 2008;37:809–815.
- [8] Pantano C, Pullin DI, Dimotakis PE, et al. LES approach for high Reynolds number wall-bounded flows with application to turbulent channel flow. *J Comput Phys*. 2008;227:9271–9291.
- [9] Chung D, Pullin DI. Large-eddy simulation and wall modelling of turbulent channel flow. *J Fluid Mech*. 2009;631:281–309.
- [10] Chung D, McKeon BJ. Large-eddy simulation of large-scale structures in long channel flow. *J Fluid Mech*. 2010;661:341–364.
- [11] Chen S, Xia Z, Pei S, et al. Reynolds-stress-constrained large-eddy simulation of wall-bounded turbulent flows. *J Fluid Mech*. 2012;703:1–28.
- [12] Yang XIA, Sadique J, Mittal R, et al. Integral wall model for large eddy simulations of wall-bounded turbulent flows. *Phys Fluids*. 2015;27(2):025112/1–025112/32.
- [13] Heinz S. *Statistical mechanics of turbulent flows*. Berlin: Springer-Verlag; 2003.
- [14] Heinz S. Unified turbulence models for LES and RANS, FDF and PDF simulations. *Theoret Comput Fluid Dynam*. 2007;21(2):99–118.
- [15] Heinz S. Realizability of dynamic subgrid-scale stress models via stochastic analysis. *Monte Carlo Methods Applic*. 2008;14(4):311–329.
- [16] Heinz S, Gopalan H. Realizable versus non-realizable dynamic subgrid-scale stress models. *Phys Fluids*. 2012;24(11):115105/1–115105/23.
- [17] Gopalan H, Heinz S, Stöllinger M. A unified RANS-LES model: computational development, accuracy and cost. *J Comput Phys*. 2013;249:249–279.

- [18] Mokhtarpoor R, Heinz S, Stoellinger M. Dynamic unified RANS-LES simulations of high Reynolds number separated flows. *Phys Fluids*. 2016;28(9):095101/1–095101/36.
- [19] Mokhtarpoor R, Heinz S. Dynamic large eddy simulation: stability via realizability. *Phys Fluids*. 2017;29(10):105104/1–105104/22.
- [20] Heinz S. The large eddy simulation capability of Reynolds-averaged Navier-Stokes equations: analytical results. *Phys Fluids*. 2019;31(2):021702/1–021702/6.
- [21] Buschmann MH, Gad el Hak M. Turbulent boundary layers: is the wall falling or merely wobbling?. *Acta Mech*. 2011;218(3-4):309–318.
- [22] Morrison JF. The interaction between inner and outer regions of turbulent wall-bounded flow. *Phil Trans R Soc A*. 2007;365(1852):683–698.
- [23] Priyadarshana PJA, Klewicki JC. Study of the motions contributing to the Reynolds stress in high and low Reynolds number turbulent boundary layers. *Phys Fluids*. 2004;16(12):4586–4600.
- [24] Klewicki JC. Reynolds number dependence, scaling, and dynamics of turbulent boundary layers. *J Fluids Eng*. 2010;32(9):094001/1–094001/48.
- [25] Heinz S. On mean flow universality of turbulent wall flows. I. High Reynolds number flow analysis. *J Turbul*. 2018;19(11-12):929–958.
- [26] Lee M, Moser RD. Direct numerical simulation of turbulent channel flow up to $Re_\tau = 5200$. *J Fluid Mech*. 2015;774:395–415.
- [27] Available from: <http://turbulence.ices.utexas.edu>, 2016.
- [28] Chin C, Monty JP, Ooi A. Reynolds number effects in DNS of pipe flow and comparison with channels and boundary layers. *Int J Heat Fluid Flow*. 2014;45:33–40.
- [29] Sillero JA, Jiménez J, Moser RD. One-point statistics for turbulent wall-bounded flows at Reynolds numbers up to $\delta^+ \approx 2000$. *Phys Fluids*. 2013;25(10):105102/1–105102/16.
- [30] Available from: <http://torroja.dmt.upm.es/turbdata/blayers>, 2016.
- [31] Schultz MP, Flack KA. Reynolds-number scaling of turbulent channel flow. *Phys Fluids*. 2013;25(2):025104/1–025104/13.
- [32] Hultmark M, Vallikivi M, Bailey SCC, et al. Logarithmic scaling of turbulence in smooth-and rough-wall pipe flow. *J Fluid Mech*. 2013;728:376–395.
- [33] Available from: <https://smits.princeton.edu/superpipe-turbulence-data>, 2016.
- [34] Vallikivi M, Hultmark M, Smits AJ. Turbulent boundary layer statistics at very high Reynolds number. *J Fluid Mech*. 2015;779:371–389.
- [35] Lozano-Durán A, Jiménez J. Effect of the computational domain on direct simulations of turbulent channels up to $Re_\tau = 4200$. *Phys Fluids*. 2014;26(1):011702/1–011702/8.
- [36] Available from: <http://torroja.dmt.upm.es/channels/data>, 2016.
- [37] Ahn J, Lee JH, Lee J, et al. Direct numerical simulation of a 30R long turbulent pipe flow at $Re_\tau = 3008$. *Phys Fluids*. 2015;27(6):065110/1–065110/14.
- [38] Schlatter P, Örlü R. Assessment of direct numerical simulation data of turbulent boundary layers. *J Fluid Mech*. 2010;659:116–126.
- [39] Available from: <http://www.mech.kth.se/pschlatt/data/readme.html>, 2016.
- [40] Townsend AA. The structure of turbulent shear flow. 1st ed. Cambridge: Cambridge University Press; 1956.
- [41] Townsend AA. Equilibrium layers and wall turbulence. *J Fluid Mech*. 1961;11:97–120.
- [42] Townsend AA. The structure of turbulent shear flow. 2nd ed. Cambridge: Cambridge University Press; 1976.
- [43] McNaughton KG, Brunet Y. Townsend's hypothesis, coherent structures and Monin-Obukhov similarity. *Bound-Layer Meteorol*. 2002;102(2):161–175.
- [44] Yamamoto Y, Tsuji Y. Numerical evidence of logarithmic regions in channel flow at $Re_\tau = 8000$. *Phys Rev Fluids*. 2018;3(1):012602/1–012602/10.
- [45] Pope SB. Turbulent flows. Cambridge: Cambridge University Press; 2000.
- [46] Kim J. Progress in pipe and channel flow turbulence, 1961–2011. *J Turbul*. 2012;13(45):1–19.
- [47] Marusic I, Monty JP, Hultmark M, et al. On the logarithmic region in wall turbulence. *J Fluid Mech*. 2013;716:R3/1–R3/11.

- [48] Abe H, Antonia RA. Relationship between the energy dissipation function and the skin friction law in a turbulent channel flow. *J Fluid Mech.* 2016;798:140–164.
- [49] Krogstad P-Å, Antonia RA. Surface roughness effects in turbulent boundary layers. *Exp Fluids.* 1999;27(5):450–460.
- [50] Marusic I, Kunkel GJ. Streamwise turbulence intensity formulation for flat-plate boundary layers. *Phys Fluids.* 2003;15(8):2461–2464.
- [51] Kunkel GJ, Marusic I. Study of the near-wall-turbulent region of the high-Reynolds-number boundary layer using an atmospheric flow. *J Fluid Mech.* 2006;548:375–402.
- [52] Marusic I, Hutchins N. Study of the log-layer structure in wall turbulence over a very large range of Reynolds number. *Flow Turbulence Combust.* 2008;81(1-2):115–130.
- [53] McKeon BJ. The engine behind (wall) turbulence: perspectives on scale interactions. *J Fluid Mech.* 2017;817:P1/1–P1/86.
- [54] Dean RB. Reynolds number dependence of skin friction and other bulk flow variables in two-dimensional rectangular duct flow. *J Fluids Eng.* 1978;100(2):215–223.
- [55] Zanon E-S, Nagib H, Durst F. Refined c_f relation for turbulent channels and consequences for high-Re experiments. *Fluid Dyn Res.* 2009;41(2):021405.